



RESEARCH

Open Access



# Functional non-glutaraldehyde treated porcine pericardium for anti-coagulation, anti-calcification, and endothelial proliferation bioprosthetic heart valves

Xiaotong Chen<sup>1,2</sup>, Tao Yu<sup>2</sup>, Qunshou Kong<sup>2</sup>, Dajun Kuang<sup>3</sup>, Hong Xu<sup>2</sup>, Zhiyu Zhao<sup>2</sup>, Li Yang<sup>2</sup>, Gaocan Li<sup>2\*</sup> , Haojun Fan<sup>1\*</sup> and Yunbing Wang<sup>2\*</sup> 

## Abstract

In the last decade, the number of transcatheter heart valve replacement for severe heart valve disease has increased exponentially. Although the bioprosthetic artificial heart valve (BHV) has similar fluid dynamics performance to the original heart valve compared with mechanical heart valve so that there is no need to take long-term anticoagulant drugs to prevent thromboembolism, transcatheter BHV replacement are still at risk for thrombosis during the first few months according to the clinical data. However, the use of antithrombotic drugs can also increase the risk of bleeding. Therefore, it is particularly important to improve the anticoagulant properties for the BHV itself. In this work, a kind of non-glutaraldehyde cross-linked BHV material with excellent antithrombotic ability has been prepared from carboxylated oxazolidine treated porcine pericardium (consisting of collagen, elastin and glycoprotein) with the further graft of the anticoagulant heparin sodium via hydrophilic modified chitosan. Along with the similar mechanical properties and collagen stability comparable to the glutaraldehyde cross-linked porcine pericardium (PP), these functional non-glutaraldehyde cross-linked PPs exhibit better biocompatibility, promoted endothelial proliferation and superior anti-calcification ability. More importantly, excellent anticoagulant activity can be observed in the hematological experiments in vivo and in vitro. In summary, these excellent performances make these functional non-glutaraldehyde cross-linked PPs great potentialities in the BHV applications.

**Keywords** Bioprosthetic heart valves, Oxazolidine, Cytocompatibility, Anti-coagulation

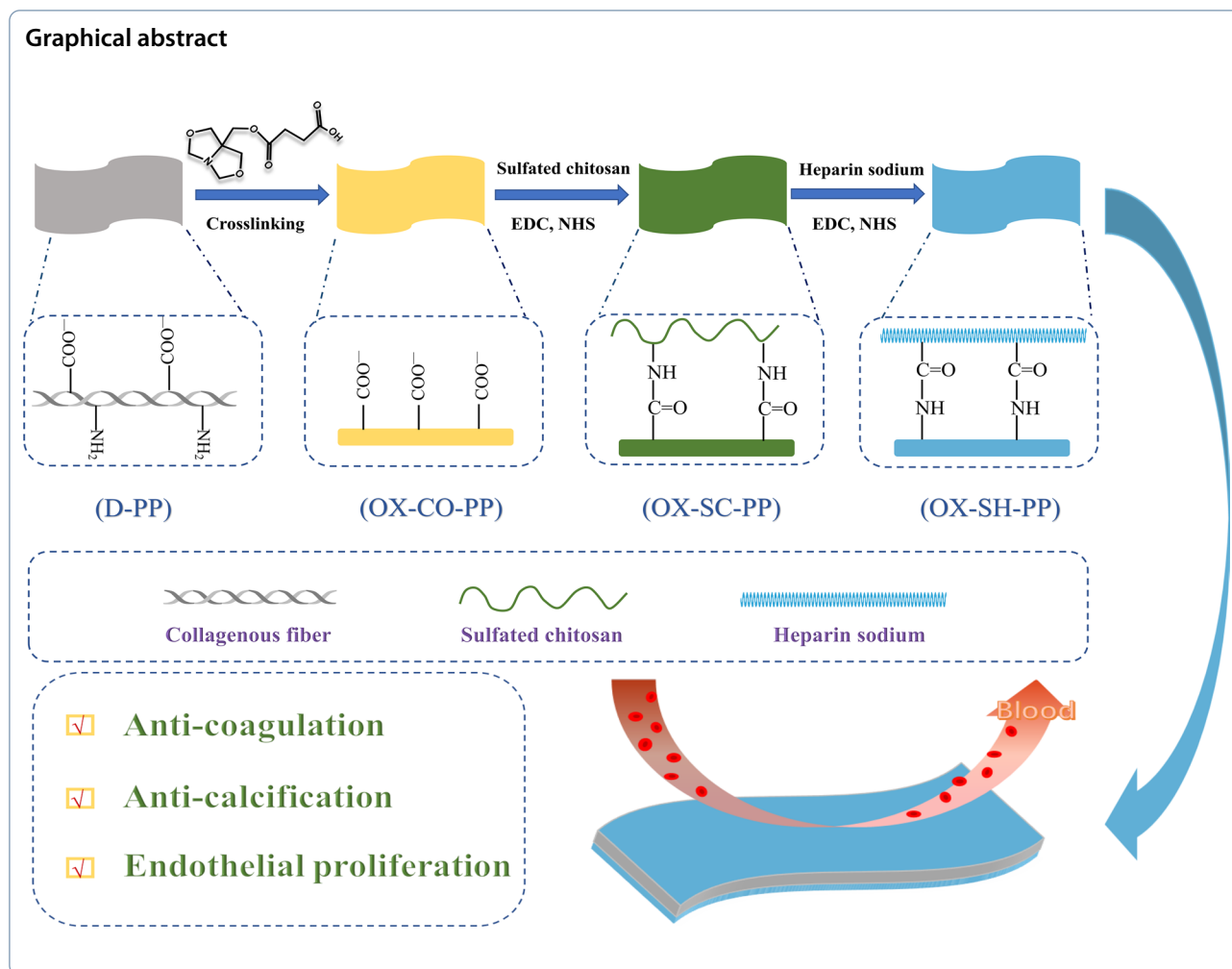
\*Correspondence:

Gaocan Li  
gaocanli@scu.edu.cn  
Haojun Fan  
fanhaojun@scu.edu.cn  
Yunbing Wang  
yunbing.wang@scu.edu.cn

Full list of author information is available at the end of the article



© The Author(s) 2022, corrected publication 2023. **Open Access** This article is licensed under a Creative Commons Attribution 4.0 International License, which permits use, sharing, adaptation, distribution and reproduction in any medium or format, as long as you give appropriate credit to the original author(s) and the source, provide a link to the Creative Commons licence, and indicate if changes were made. The images or other third party material in this article are included in the article's Creative Commons licence, unless indicated otherwise in a credit line to the material. If material is not included in the article's Creative Commons licence and your intended use is not permitted by statutory regulation or exceeds the permitted use, you will need to obtain permission directly from the copyright holder. To view a copy of this licence, visit <http://creativecommons.org/licenses/by/4.0/>.



## 1 Introduction

Heart valve replacement is a first-line treatment for severe heart valve diseases [1, 2]. The transcatheter heart valve replacement provides a new option and has gradually become a mainstream treatment method due to its advantages such as no requirement of thoracotomy, short operation time, minimally invasion, relatively low risk, and rapid postoperative recovery [3, 4]. Compared with mechanical heart valves, bioprosthetic heart valves (BHV) are favored by the patients who might be at risk of surgical bleeding (such as the elderly, the pregnant women and so on) due to its excellent hydrodynamic property and no need for lifelong anticoagulation [5, 6]. At present, most of the BHV materials used in clinic are porcine pericardium (PP) or bovine pericardium (BP) crosslinked by glutaraldehyde [7, 8]. However, cytotoxicity of glutaraldehyde can cause inflammatory response and subclinical leaflet thrombosis [9, 10]. Clinical data suggests that patients who undergo transcatheter BHV replacement are

still at risk of thrombosis in the first few months post-implantation [11, 12]. Particularly, for the patients with pulmonary valve and venous valve replacement, the slow blood flow on the pulmonary valve will increase the risk of thrombosis [13]. In more severe cases, blood clots may lead to the life-threatening stroke or endocarditis [14, 15]. Thrombosis and inflammation would further promote the calcification of the valves, affecting the valve function and shortening the lifetime of BHVs [16, 17]. Therefore, it is essential to improve the antithrombotic feature along with the anti-calcification property to enhance the comprehensive performance for BHVs [18].

Heparin sodium is an antithrombotic drug commonly used in clinic [19]. Immobilizing heparin to the BHVs is proved to be a good choice to promote antithrombotic property [20, 21]. Heparin could be mixed with fresh pericardium and then crosslinked by glutaraldehyde to obtain the heparin modified BHVs [22]. However, this method would lock up the spatial structure

of heparin and greatly reduce the biological activity of heparin [20]. Meanwhile, the grafting of heparin to the surface of the cross-linked pericardium rather than fresh pericardium is also studied [23, 24]. There is little amino group remained for the pericardium after crosslinking reaction. The difficulty of surface modification of heparin on cross-linked pericardium lies in how to improve the graft density of heparin. Increasing the amino groups on the surface of cross-linked pericardium with an intermediate can be viable. But the highly positively charged of the intermediates such as polyethyleneimine or chitosan are susceptible to cause the severe blood clotting [25, 26]. Therefore, choosing a suitable intermediate is important. Sulfated chitosan, a derivative of chitosan with antithrombotic effect [27], can be a potential option to provide a large number of active amino groups along with excellent anticoagulant, antiviral properties and biocompatibility [27].

A series of non-glutaraldehyde cross-linked BHV materials with good biocompatibility and reduced calcification have been developed by us by the treatment of PP cross-linked with the bicyclic oxazolidines [28, 29]. Meanwhile, the mechanical property and collagen stability of these oxazolidine cross-linked PP are comparable to those of the glutaraldehyde cross-linked PP, and the BHV made from the oxazolidine cross-linked PP exhibit good durability in the accelerated fatigue test with more than 350 million cycles. However, the further improvement of the antithrombotic property for these oxazolidine cross-linked PP is still needed. In this work, the heparin sodium grafted cross-linked PP (OX-SH-PP) has been developed through the cross-linking of PP by a designed bicyclic oxazolidine (OX-CO) with a carboxyl functional group and the subsequent graft of the anticoagulant heparin sodium onto the oxazolidine cross-linked PP via the bridge of sulfated chitosan. The antithrombotic performance of OX-SH-PP was evaluated systematically through *in vitro* and *ex vivo* tests. The physical and chemical properties, mechanical properties, ability to resist enzyme degradation resistance, biological safety, anti-calcification property and endothelial cells proliferation of OX-SH-PP are further studied.

## 2 Materials and methods

Fresh porcine pericardium (PP) was obtained by Venus Medtech Inc (Hangzhou, China). Trimethylaminomethane (Tris) were obtained from Chengdu Best Reagent Co. Ltd (Chengdu, China). Heparin sodium was purchased from Macklin Biochemical Co., Ltd (Shanghai, China). Low molecular weight chitosan with a degree of deacetylation of 0.75~0.85 was purchased from Sigma Aldrich

(Shanghai, China). Dulbecco's modified eagle medium (DMEM), fetal bovine serum (FBS) and phosphate buffered saline (PBS) were brought from Gibco (Thermo Fisher Scientific, US). Cell Counting Kit-8 (CCK-8) was purchased from Beyotime Biotechnology Co. Ltd (Shanghai, China). TRITC-phalloidin and collagenase were purchased from Solarbio Life Sciences Co. Ltd (Beijing, China). OX-OH was synthesized according to the reported literature [30]. 3,6-*O*-sulfated chitosan was prepared according to the previously reported method[31].

### 2.1 Synthesis of OX-CO

Hydroxymethyl oxazolidine (OX-OH) (24.00 g, 165.5 mmol) and succinic anhydride (18.10 g, 179.8 mmol) were dissolved in dry tetrahydrofuran (100 mL). After refluxing at 130 °C for 8 h, the white crystal was obtained by rotary evaporation and purified by recrystallization as the same method above. The product OX-CO was successfully prepared (28.00 g, 69%), <sup>1</sup>H NMR (400 MHz, CDCl<sub>3</sub>) δ=9.94 (s, 1H), 4.49 (dd, *J*=25.0 Hz, 5.5 Hz, 4H), 4.20 (s, 2H), 3.90–3.73 (m, 4H), 2.88–2.54 (m, 4H) ppm. <sup>13</sup>C NMR (100 MHz, CDCl<sub>3</sub>) δ=177.0, 171.8, 88.0, 73.7, 71.3, 66.5, 28.8 ppm. MS (ESI +): calculated for C<sub>10</sub>H<sub>16</sub>NO<sub>6</sub> [M+H]<sup>+</sup> 246.10, found 246.07.

### 2.2 Preparation of decellularized porcine pericardium (D-PP)

Fresh PP was decellularized according to the method described in a previous report [32, 33]. Fresh PP was incubated with the acellular solution containing 0.5% sodium dodecyl sulfonate and 0.5% sodium deoxycholate with oscillating for 12 h. Then, the resulting decellularized porcine pericardium (D-PP) was rinsed by distilled water for 2 h under shaking every time. After washing for 5 times, the D-PP was stored in PBS solution for the subsequent experiment.

### 2.3 Preparation of glutaraldehyde cross-linked PP (G-PP)

The D-PP was attached to a 5 cm × 5 cm square frame for subsequent crosslinking reaction. Then the D-PP was treated with glutaraldehyde solution (0.625%, wt%) for 72 h. After the crosslinking process, the resulting PP was stored in glutaraldehyde solution (0.5%, wt%).

### 2.4 Preparation of OX-CO cross-linked PP (OX-CO-PP)

The D-PP was immersed into different concentrations of OX-CO solution (1%, 3%, 5% and 7%, wt%) and oscillated for 72 h. The OX-CO-PP was prepared and then thoroughly washed by distilled water (as described in 2.2), and stored in 75% ethanol.

### 2.5 Preparation of sulfated chitosan grafted cross-linked PP (OX-SC-PP)

The OX-CO-PP was incubated with carboxyl-group-activated solution consisting of NHS (0.1 M) and EDC (0.1 M) [34]. After stirring for 2 h, 3,6-*O*-sulfated chitosan (1%, wt%) was added and oscillated for 24 h. Then the resulting PP was thoroughly washed with distilled water (as described in 2.2), and the OX-CO cross-linked PP grafted with sulfated chitosan (OX-SC-PP) was obtained and stored in 75% ethanol.

### 2.6 Preparation of heparin sodium grafted cross-linked PP (OX-SH-PP)

Heparin sodium (1%, wt%) was activated by NHS (0.1 M) and EDC (0.1 M) for 2 h. Then the OX-SC-PP was incubated with the resulting solution for 24 h [34]. And then, the resulting PP was thoroughly washed with distilled water (as described in 2.2), and the OX-CO cross-linked porcine pericardium grafted with heparin sodium by sulfated chitosan (OX-SH-PP) was successfully prepared and stored in 75% ethanol.

### 2.7 The measurement of free amine group

The free amine group of the cross-linked PP was quantified via ninhydrin assay [35]. In brief, the D-PP, G-PP or OX-CO-PP (around 1 cm × 1 cm size) was weighed respectively. Each sample was put into a centrifuge tube containing 1 mL ninhydrin working solution consisting of 50% v/v ninhydrin (1% W/V) in sodium citrate (0.1 M, pH=5) and 50% V/V diethylene glycol monomethyl ether, and then was heated to 95 °C in a water bath for 20 min. 250 μL of isopropanol aqueous solution (50%, V/V) was added to each sample after the resulting solution cooled down. 100 μL of the supernatant solution was drawn into the 96-well plate and measured at 567 nm by using microplate reader. The results were calculated according to the following formula:

$$\text{Conversion of amine group} = 1 - \frac{\frac{A_{\text{sample}}}{W_{\text{sample}}}}{\frac{A_{\text{D-PP}}}{W_{\text{D-PP}}}} \times 100\%$$

where  $A_{\text{sample}}$  is the measured absorbance of cross-linked PPs,  $W_{\text{sample}}$  is the weight of cross-linked PPs,  $A_{\text{D-PP}}$  is the measured absorbance of D-PP, and  $W_{\text{D-PP}}$  is the weight of D-PP.

### 2.8 Thermal shrinkage temperature measurement

Thermal shrinkage temperature was determined by differential scanning calorimetry (DSC). Samples were cut into 1 cm × 1 cm size after freeze-drying. The heating curve was acquired by DSC 2920 (TA Instruments,

Newcastle, DE) under the conditions including N<sub>2</sub> atmosphere and a heating rate of 10 °C/min.

### 2.9 Microscopic morphology observation

The crosslinked PP samples were cut into 12 mm diameter disks and freeze-dried. The micromorphology was observed by scanning electron microscopy (SEM, JEOL, JSM-7500F, Japan) after gold sputtering.

### 2.10 Uniaxial tensile testing

The sample was cut into 40 mm × 10 mm along the fiber direction, and the thickness of the three points was measured randomly with a thickness tester. The tensile test was carried out with a uniaxial tensile tester with a tensile speed was 12.5 mm/min. The ultimate tensile strength, elongation, tangent modulus and extensibility were calculated by previously reported methods [36].

### 2.11 Collagenase and elastase degradation

The cross-linked and uncross-linked samples were lyophilized and weighed after being cut into 1 cm × 1 cm size. The samples were incubated with 1 mL collagenase or elastase solution with a concentration of 1 mg/mL (125 U/mL) for 24 h at 37 °C. The samples were thoroughly washed with distilled water, and finally freeze-dried and weighed. The weight before and after enzymatic hydrolysis were named as  $W_0$  and  $W_1$ , respectively.

$$\text{Weight loss rate} = \frac{W_0 - W_1}{W_0} \times 100\%$$

### 2.12 Cytotoxicity evaluation

Cytotoxicity of materials was evaluated according to the methods described in the national standard. To put it simply, the cross-linked PPs were sterilized with 75% ethanol and then extracted in DMEM medium (6 cm<sup>2</sup>/mL, superficial area/volume) at 37 °C for 72 h. The L929 cells were digested with 0.25% trypsin and planted in a 96-well plate at a density of 5000 cells/well. After incubation for 24 h, 100 μL material extract was added to replace the original medium for 24 or 48 h. The cell activity was measured by CCK-8 kit.

### 2.13 Endothelial cell adhesion and proliferation

The cross-linked PP was cut into disks with a diameter of 12 mm, placed in a 48-well plate and sterilized as the same method in cytotoxicity evaluation. The well-growing human endothelial cells were digested and then the samples were immersed at a density of 20,000 cells/well. After incubation for 24 or 48 h, the samples were transferred to a new 48-well plate, washed with PBS, fixed with 2.5% glutaraldehyde fixing solution and labeled with

TRITC-phalloidin and DAPI, respectively. Cell morphology on the cross-linked PPs was observed under a confocal laser microscope (Zeiss LSM 800, DE).

#### 2.14 Hemolysis rate determination

The rabbit blood extracted from the middle auricle artery was centrifuged at 1000 rpm for 15 min. The upper serum was discarded and the lower red blood cells were left. The blood was diluted 10 times with PBS solution. The crosslinked PP was cut into a circle with a diameter of 10 mm, placed in a 1.5 mL centrifuge tube, and infiltrated with 200  $\mu$ L PBS solution. Ultrapure water and PBS solution were used as positive control and negative control, respectively. Diluted red blood cells (800  $\mu$ L) were added to each well and incubated for 24 h. The cross-linked PP was removed and centrifuged. The absorbance of the supernatant at 545 nm was tested by a microplate reader.

#### 2.15 Coagulation experiment in the whole blood

The cross-linked PP was made into circular plates with a diameter of 10 mm, placed in a 48-well plate, and thoroughly cleaned with PBS. Fresh rabbit blood was centrifuged at 3000 rpm for 15 min, and the upper frequency platelet plasma (FPP) was taken out. FPP (500  $\mu$ L) was added to each well and incubated for 90 min at 37 °C. After incubation, the serum was analyzed for prothrombin time (PT) and activated partial thrombin time (APTT) by a semi-automatic hematology-analyzer.

#### 2.16 Recalcification whole blood clotting experiment

3% (V/V)  $\text{CaCl}_2$  (100 mM) was added to the newly collected blood from rabbit to prepare the recalcified blood. The cross-linked PP was shaped into a round plate with a diameter of 6 mm and then placed in a 96-well plate. Recalcified blood (200  $\mu$ L) was added and incubated for 10 min at 37 °C. Then the resulting samples were transferred to a new 96-well plate and cleaned it with PBS for 3 times. 300  $\mu$ L TritonX-100 (0.5%, V/V) was added to each sample to dissolve thrombus. The absorbance of the supernatant was measured at 405 nm by a microplate analyzer.

#### 2.17 Ex vivo arteriovenous shunt (AV-shunt) assay

The use of animals and all protocols were approved by the by the Sichuan Provincial Committee for Experimental Animal Management and performed according to the institutional and NIH guidelines for the care and use of research animals. The cross-linked PPs were cut into rectangles of 10 mm  $\times$  15 mm, washed with sterile PBS after sterilization (the same as the cytotoxicity evaluation method), and placed in a catheter of about 2 mm in diameter. The blank group was an empty catheter without cross-linked PPs. New Zealand white rabbits (around

3 kg) were anesthetized with 2% sodium pentobarbital at a dose of 30 mg/kg and injected with 100 U/kg heparin sodium before operation. The skin and muscle of the rabbit's neck were cut open, and the carotid artery and jugular vein were externally connected through a catheter to establish blood circulation. Two hours later, the catheter was pulled out and cleaned with normal saline. The sample weights  $W_1$  (before the operation) or  $W_2$  (after the operation) were recorded. The thrombus was fixed with 2.5% glutaraldehyde fixation solution for 1 h, then dehydrated with gradient ethanol and dried. The thrombus was observed by SEM (JSM-5900LV, JEOL, Japan).

$$\text{Thrombogenesis} = W_2 - W_1$$

#### 2.18 Complement activation measurement

The cross-linked PPs were divided into disks with a diameter of 10 mm and placed in a 48-well plate. Then they were immersed in plasma separated from 500  $\mu$ L whole blood via centrifugation (the same as the coagulation test). The plasma was oscillated at 37 °C for 1 h. The resulting plasma was collected and determined with the C3a enzyme immunoassay kit.

#### 2.19 Ubcutaneous implantation

The cross-linked PPs were cut into 1 cm  $\times$  1 cm and thoroughly rinsed with sterile PBS after sterilization. SD rats (100 g  $\pm$  10 g) were anesthetized by intraperitoneal injection of 2% pentobarbital sodium at a dose of 30 mg/kg. The hair on the back was shaved, and back skin was disinfected with wiping povidone-iodine solution. Two holes (about 1 cm) were cut in the middle and two pockets were opened on both sides. The crosslinked PPs were placed in the pocket and sutured. Samples were taken out at 7, 30 and 60 days respectively. Some of the samples were weighed after being freeze-dried and heated with concentrated nitric acid in a water bath at 100 °C until all the solids were dissolved. The calcium content was analyzed by ICP-AES. The other part was fixed with 4% paraformaldehyde, gradient dehydrated, embedded, sectioned and stained for HE, immunohistochemistry and alizarin red. The numbers of CD3-positive cells and CD68-positive cells were counted by Image pro plus.

### 3 Results and discussion

#### 3.1 Preparation of OX-CO-PP, OX-SC-PP and OX-SH-PP

As shown in Additional file 1: Fig. S1, bicyclic oxazolidine OX-CO with a more reactive carboxyl functional group was synthesized through the esterification reaction of hydroxyl group of OX-OH with succinic anhydride to providing more versatility for material preparation and properties [37]. The chemical structure of OX-CO was characterized by  $^1\text{H}$  NMR,  $^{13}\text{C}$  NMR and MS. These

results shown in Additional file 1: Fig. S1, S2 indicated that OX-CO was successfully prepared.

With the functional crosslinking agent OX-CO in hand, OX-CO-PP was obtained by the treatment of D-PP with OX-CO. According to the amine conversion of different concentrations of OX-CO-PPs (Additional file 1: Fig. S3), the working concentration of OX-CO was finally selected as 3% (wt%) for cross-linking of PP. With a large number of carboxyl groups remained on OX-CO-PP, the modification of OX-CO-PP with sulfated chitosan was conducted through the chemical linkage of amide groups to obtain OX-SC-PP, following with the further grafting of heparin sodium with sulfated chitosan to achieve the functional BHV material OX-SH-PP. Sulfated chitosan could not only provided a lot of amine groups, but also cooperated with heparin sodium in anti-coagulation. According to the standard curve of sulfated chitosan and heparin sodium (Additional file 1: Fig. S5), the grafting degree of sulfated chitosan and heparin sodium were calculated to be  $31.57 \pm 1.32 \mu\text{g}/\text{cm}^2$  and  $43.93 \pm 15.32 \mu\text{g}/\text{cm}^2$ , respectively.

### 3.2 Thermodynamic and biochemical stability and mechanical property

The morphology and orientation of valve fibers are closely related to the mechanical properties and anti-degradation properties. The morphologies of D-PP, OX-CO-PP, OX-SC-PP and OX-SH-PP were shown in Additional

file 1: Fig. S6. The collagen fibers of D-PP were loosened in the sample preparation for SEM, while the gaps were decreased and the surface was more compact for these cross-linked PPs (Fig. 1). The thermal shrinkage temperature can be used to characterize the stability of collagen materials. As shown in Fig. 2A, the thermal shrinkage temperature of G-PP ( $88.4 \text{ }^\circ\text{C} \pm 3.51 \text{ }^\circ\text{C}$ ) was significantly higher than that of D-PP ( $77.27 \text{ }^\circ\text{C} \pm 1.62 \text{ }^\circ\text{C}$ ). The DSC of OX-CO-PP ( $93.11 \text{ }^\circ\text{C} \pm 1.17 \text{ }^\circ\text{C}$ ) was higher than that of G-PP. This result indicated OX-CO could significantly stabilize PP materials. What's more, the thermal shrinkage temperature of OX-SH-PP ( $96.67 \text{ }^\circ\text{C} \pm 3.67 \text{ }^\circ\text{C}$ ) was slightly higher than that of OX-CO-PP, which might be caused by hydrogen bonding after the graft of sulfated chitosan and heparin sodium [38].

PP is mainly composed of collagen and elastin. After the treatment of collagenase (Fig. 2B), the weight loss rate of the D-PP, G-PP, OX-CO-PP and OX-SH-PP was 93.69%, 2.73%, 7.06% and 1.73%, respectively. After the treatment of elastase (Fig. 2C), the weight loss rate of the D-PP, G-PP, OX-CO-PP and OX-SH-PP was 17.36%, 7.32%, 7.38% and 7.32%, respectively. Since chemical crosslinking could greatly improve collagen stability, collagenase degradation resistance could be observed for these cross-linked PPs. However, the elastin is mainly composed of nonpolar amino acids (Gly, Val, Ala, Pro and so on), which cannot be crosslinked by OX-CO,

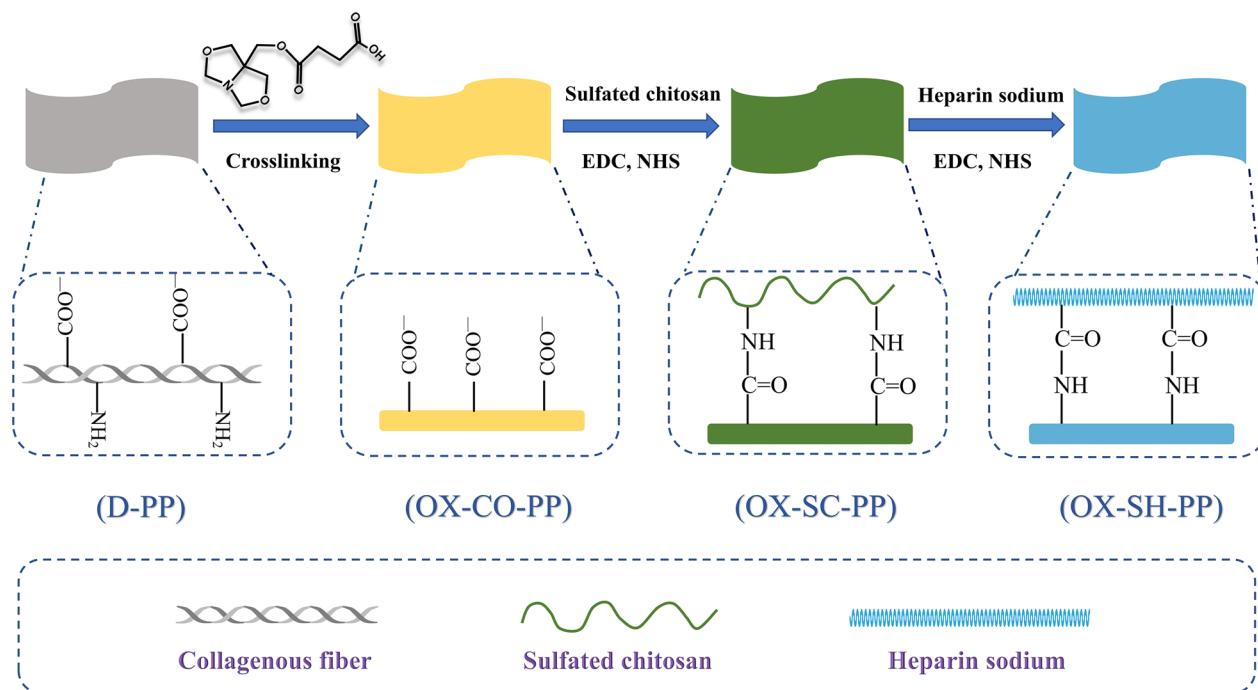


**Fig. 1** The prepared route of OX-CO-PP, OX-SC-PP and OX-SH-PP

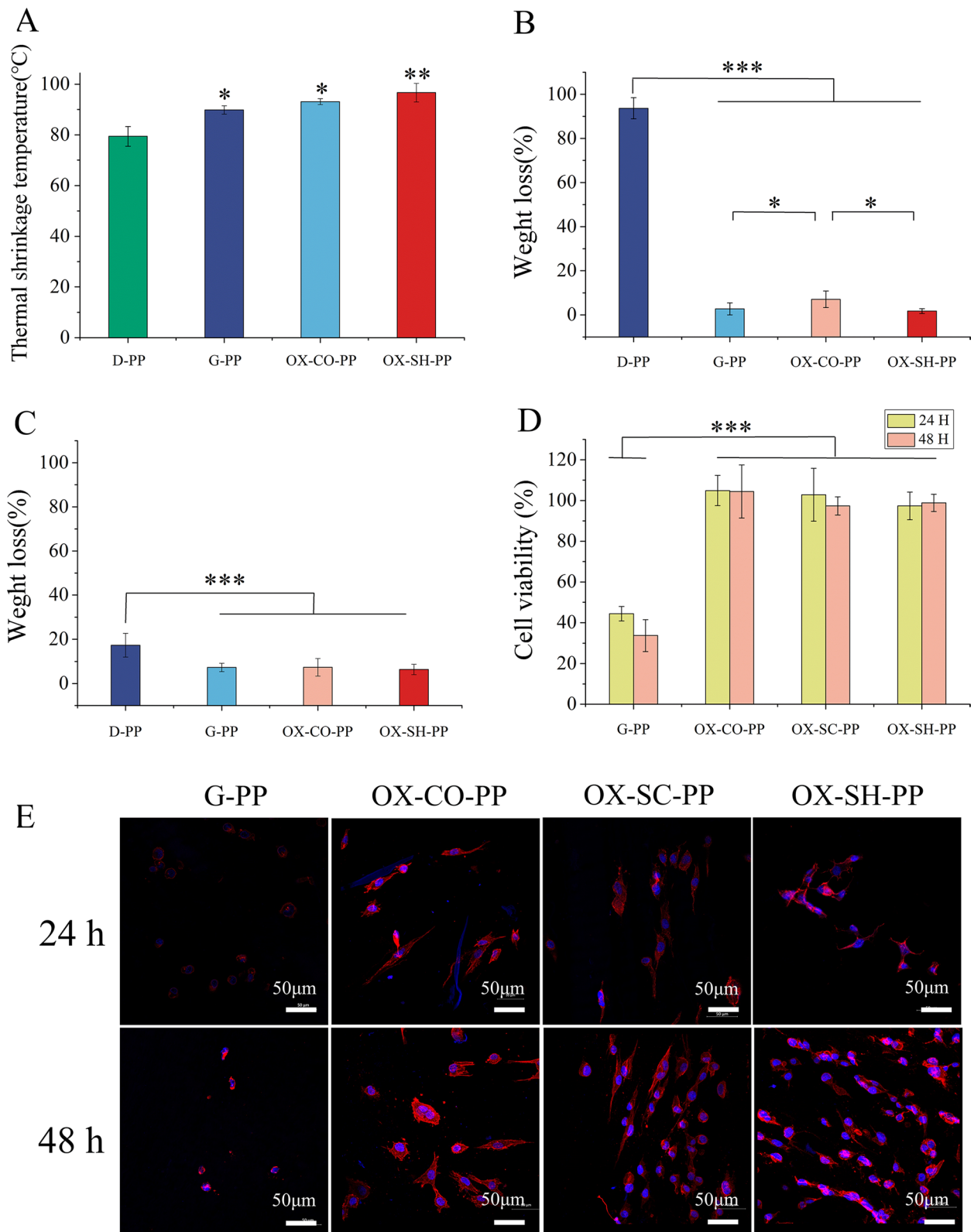


**Fig. 2** **A** The thermal shrinkage temperature of D-PP or crosslinking PP (n = 3). Resistance to collagenase **B** or elastase **C** degradation. **D** Cell viability assessment after incubated with the extraction medium of PPs for 24 h or 48 h. **E** Observation of adhesion of HUVECs to the valves after 24 h and 48 h growth by TRITC-phalloidin (red) and DAPI (blue) staining. (bar = 50 μm)

**Table 1** Mechanical properties of PPs

Tissues	Ultimate tensile strength (MPa)	Elongation (%)	Tangent modulus (MPa)	Extensibility (%)
D-PP	8.63 ± 2.44	26.45 ± 3.96	49.89 ± 14.83	6.28 ± 2.01
G-PP	19.48 ± 2.42	23.61 ± 1.16	102.78 ± 9.82	6.41 ± 1.57
OX-CO-PP	19.43 ± 1.02	22.85 ± 4.63	102.83 ± 14.32	5.31 ± 2.14
OX-SC-PP	19.25 ± 1.17	22.55 ± 3.67	110.88 ± 13.56	5.85 ± 2.36
OX-SH-PP	20.21 ± 1.93	25.79 ± 2.85	102.33 ± 9.30	6.59 ± 2.03

resulting into different behavior of collagenase and elastase degradation.

Heart Valves act as one-way valves in the human body to prevent blood reflux and need to be opened and closed for hundreds of millions of times. The good mechanical strength is an essential for their long lifetime. The mechanical properties of crosslinked BHV valves were evaluated by uniaxial tensile test. As reported, Glut-treated PPs have been proved exhibit good mechanical properties. As shown in Table 1, the ultimate tensile strength of the G-PP (19.48 MPa ± 2.42 MPa), OX-CO-PP (19.43 MPa ± 1.02 MPa) and OX-SH-PP (20.21 MPa ± 1.93 MPa) were shown similar to G-PP (19.25 MPa ± 1.17 MPa), which were significantly higher than that of the D-PP (8.63 MPa ± 2.44 MPa). Meanwhile, the high tangent modulus of all cross-linked PPs (G-PP: 102.78 MPa ± 9.82 MPa; OX-CO-PP: 102.83 MPa ± 14.32 MPa; OX-SC-PP: 110.88 MPa ± 13.56 MPa and OX-SH-PP: 102.33 MPa ± 9.30 MPa) were also significantly higher than that of D-PP (49.89 MPa ± 14.83 MPa), indicating the mechanical properties for these oxazolidine treated PPs were excellent.

### 3.3 Cytotoxicity of PPs

As shown in the Fig. 2D, the viability of L929 cells treated with G-PP extract was 44.38% ± 3.53% after 24 h, and 33.71% ± 7.78% after 48 h, indicating a relatively high toxicity for G-PP. The survival rate of cells treated with OX-CO-PP, OX-SC-PP and OX-SH-PP was close to 100% whether after 24 h or 48 h. At the same time, the growth of endothelial cells in the cross-linked PPs was also observed in the Fig. 2E. There were only a few endothelial cells attached to the G-PP after 24 h or 48 h with the poor morphological phenotype and the growth condition of the cells. The cells of OX-CO-PP, OX-SC-PP and OX-SH-PP were spindle-shaped after 24 h, and the number of cells significantly increased after 48 h with normal morphological phenotype and good growth condition, indicating the good cell compatibility and the enhanced growth of endothelial cells for OX-SH-PP [39, 40].

### 3.4 Hematological evaluation in vitro

The blood compatibility and anticoagulant ability of the cross-linked valve were studied. As an implantable blood contact medical device, it is necessary to evaluate the hemolysis rate of BHV materials. As shown in Fig. 3A, the hemolysis rate of G-PP, OX-CO-PP, OX-SC-PP and OX-SH-PP was 1.41% ± 0.28%, 0.79% ± 0.32%, 0.37% ± 0.33% and 0.24% ± 0.23%, respectively, far below the acceptable hemolysis rate standard of less than 3%. In addition, prothrombin time (PT) and activated partial thrombin time (APTT) were used to evaluate the anticoagulant ability of these cross-linked PPs. As shown in Fig. 3B, there was no significant difference of the PT for all groups with values of blank control, G-PP, OX-CO-PP, OX-SC-PP, and OX-SH-PP as 8.27 s ± 0.27 s, 8.18 s ± 0.12 s, 8.03 s ± 0.08 s, 8.28 s ± 0.15 s and 9.03 s ± 0.75 s, respectively. While the APTT of blank control, G-PP and OX-CO-PP were 17.2 s ± 2 s, 20.7 ± 0.34 s and 20.35 ± 0.77 s, respectively, the APTT of OX-SC-PP with 50.52 s ± 1.92 s and OX-SH-PP with 110.65 s ± 12.69 s was shown, with 2.94 times and 6.43 times higher than that of blank control, respectively. The concentration of TAT was also measured via the TAT (thrombin-antithrombin complex) Elisa kit. As shown in Fig. 3C, compared to the TAT concentration of control group (191.36 pg/mL), the TAT concentration of OX-SC-PP and OX-SH-PP was 282.32 pg/mL and 393.66 pg/mL, respectively, indicating that the introduction of sulfated chitosan and heparin sodium could result into a significant enhancement of the ability of antithrombin to bind thrombin to form TAT complex [41], inhibit the activity of blood coagulation factor and prolong the APTT.

When the blood comes into contact with a foreign substance, the host's complement system will be activated and the component of components C3 will split into C3a and C3b [42]. Therefore, the level of complement activation level can be evaluated by the concentration of C3a. As shown in the Fig. 3D, the concentrations of C3a in G-PP, OX-CO-PP, OX-SC-PP and OX-SH-PP were 28.29 ng/mL, 29.59 ng/mL, 28.94 ng/mL and 30.55 ng/mL respectively, which were all lower than those in the control group (31.17 ng/mL), indicating that the low immunogenicity for these cross-linked PPs.



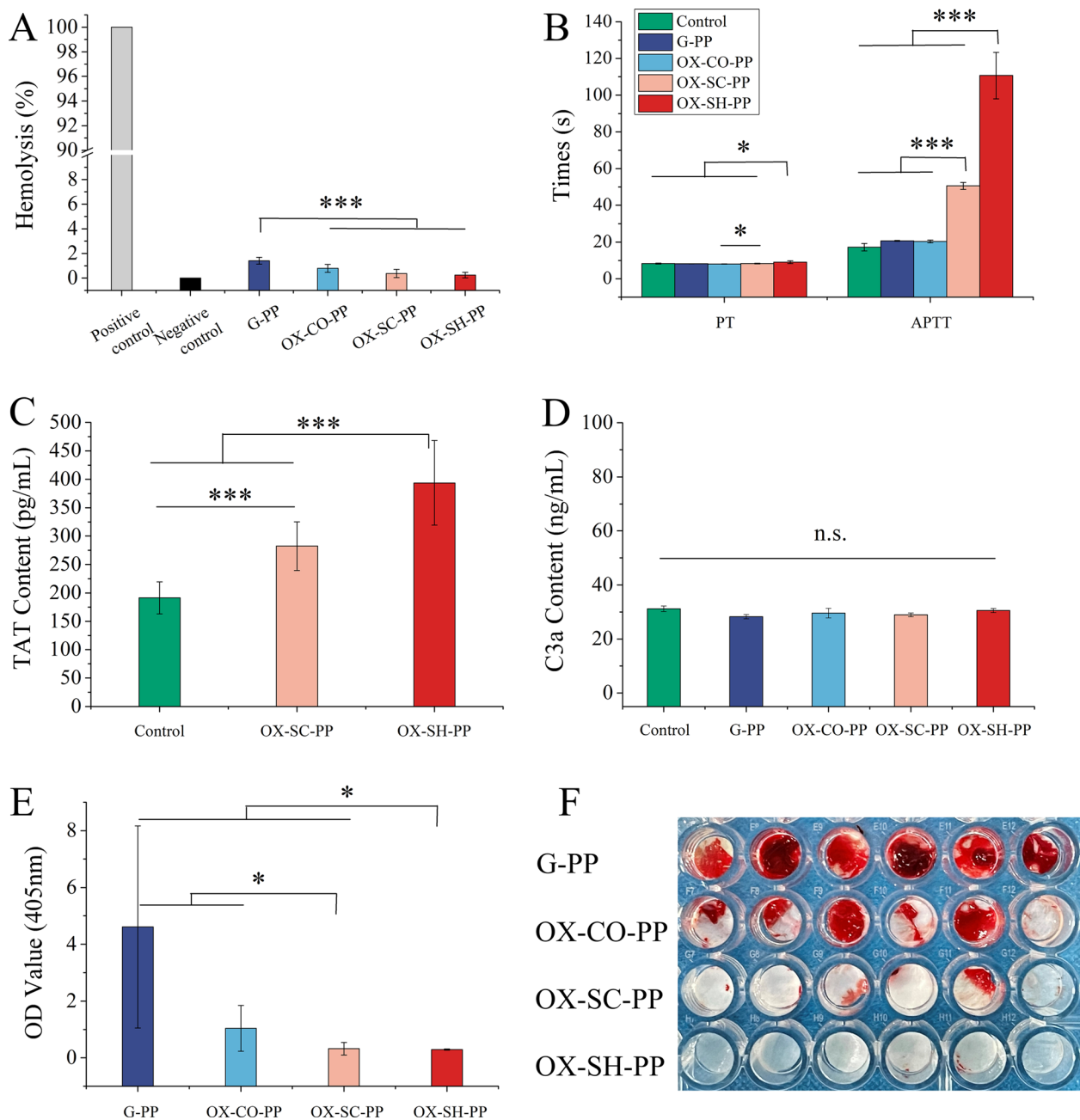


**Fig. 3** **A** Hemolysis effect of G-PP, OX-CO-PP, OX-SC-PP and OX-SH-PP; **B** APTT and PT for plasma after incubation with PPs; **C** The TAT content of plasma after incubation with PPs; **D** The concentrations of C3a in the plasma after treatment with PPs. The amount (**E**) and images **F** of thrombus generated on the surface of PPs after recalcified whole blood clotting. (\* $p < 0.05$ , \*\* $p < 0.01$ , \*\*\* $p < 0.001$ )

The antithrombotic ability of cross-linked valves in vitro was evaluated by whole blood remodification coagulation test. Figure 3F intuitively reflected the antithrombotic abilities of the four groups. After incubation with the recalcified whole blood, a large number of thrombosis formed in the G-PP group, and some thrombus formed in the OX-CO-PP group, while only a small part of thrombus formed in the OX-SC-PP and

OX-SH-PP groups. The absorbance of hemoglobin (Fig. 3E) further reflected the thrombogenic volume, demonstrating the superior antithrombotic ability for the OX-SH-PP.

The anticoagulant ability of cross-linked PPs in living blood flow was tested by *ex vivo* AV-shunt (Fig. 4A). As shown in Additional file 1: Fig. S7, 2 h after the blood flow through the catheter, there was no thrombosis in

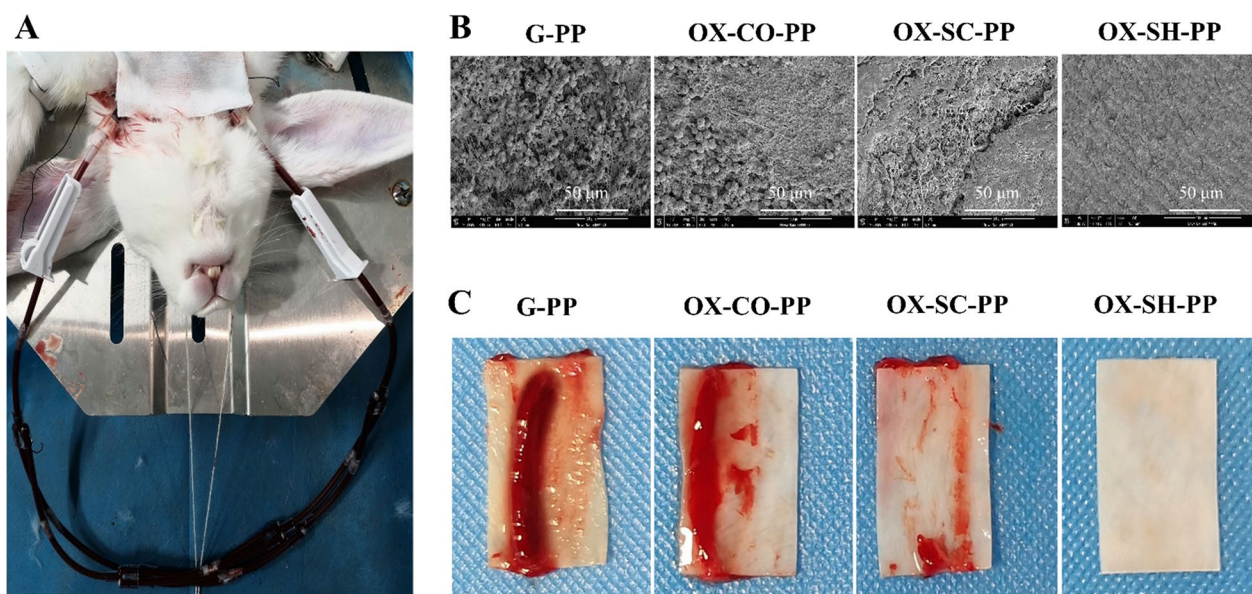


**Fig. 4** Evaluation of the hemocompatibility of G-PP, OX-CO-PP, OX-SC-PP and OX-SH-PP by *ex vivo* AV-shunt in rabbits for 2 h. **A** Illustration for AV-shunt assay. **B** SEM images of cross-linked PPs after *ex vivo* AV-shunt assay. **C** Images of cross-linked PPs after *ex vivo* AV-shunt assay

the blank group, indicating that the catheter itself did not cause coagulation. The G-PP group, OX-CO-PP group and OX-SC-PP group were all blocked. A large amount of thrombus formed in G-PP and OX-CO-PP group, and partial thrombus formed in OX-SC-PP group. In the OX-SH-PP group, the catheter was permeable and there was no obvious thrombosis. Scanning electron microscopy (Fig. 4B) showed that thrombus formation by the combination of fibrin and blood cells could be observed for G-PP, OX-CO-PP and OX-SC-PP groups, while almost no blood cells were shown on the surface of OX-SH-PP, indicating that the modification of heparin through the sulfated chitosan could successfully improve the anticoagulant ability of the cross-linked PPs.

### 3.5 Calcification analysis and immune responses

As shown in Fig. 5A, there were large amounts of dark red calcification spots on G-PP after 60 days, while no significant calcification spots were found in OX-CO-PP, OX-SC-PP and OX-SH-PP. The calcification was also quantitatively analyzed by ICP-AES. As shown in the Fig. 5B, after implantation in SD rats for 30 days, while the calcium content of G-PP was 11.45  $\mu\text{g}/\text{mg}$ , the calcium contents of OX-CO-PP (1.38  $\mu\text{g}/\text{mg}$ ), OX-SC-PP (2.79  $\mu\text{g}/\text{mg}$ ) and OX-SH-PP (1.42  $\mu\text{g}/\text{mg}$ ) were significantly lower than that of G-PP. After 60 days, the calcium content was further increased to 126.46  $\mu\text{g}/\text{mg}$ . It was worth nothing that OX-CO-PP (2.84  $\mu\text{g}/\text{mg}$ ), OX-SC-PP (3.74  $\mu\text{g}/\text{mg}$ ) and OX-SH-PP (2.41  $\mu\text{g}/\text{mg}$ ) still maintained a very low degree of calcification. The degree of

calcification was further determined by alizarin red staining section. With CD3 and CD68 as specific markers for the amounts of T-lymphocytes and macrophages respectively, the immune rejection for the cross-linked PPs after implantation was investigated by immunohistochemical staining slices. As shown in the Fig. 5C, D, compared with G-PP, there were much fewer T-lymphocyte (CD3) and macrophage (CD68) antibodies observed for OX-CO-PP, OX-SC-PP and OX-SH-PP, indicating the better biocompatibility for these oxazolidine cross-linked PPs. The reported studies have shown that the calcification is related to a variety of factors for G-PP such as residual aldehyde groups and inflammation reaction. The ability of good anti-calcification property for non-glutaraldehyde cross-linked PPs might be attributed to their good biocompatibility, absence of aldehyde residue after cross-linking, and low inflammatory response.

## 4 Conclusion

In this study, functional BHV materials with excellent anticoagulant properties have been developed based on non-glutaraldehyde cross-linked PPs. Excellent anticoagulant properties have been shown for these functional oxazolidine cross-linked PPs, which is a promising attempt for BHV replacements in the slow blood flow conditions such as pulmonary valve and venous valve replacement. Meanwhile, compared with glutaraldehyde treated PPs, better biocompatibility, superior anticoagulant ability, reduced calcification and promoted endothelial adhesion have also been demonstrated for these

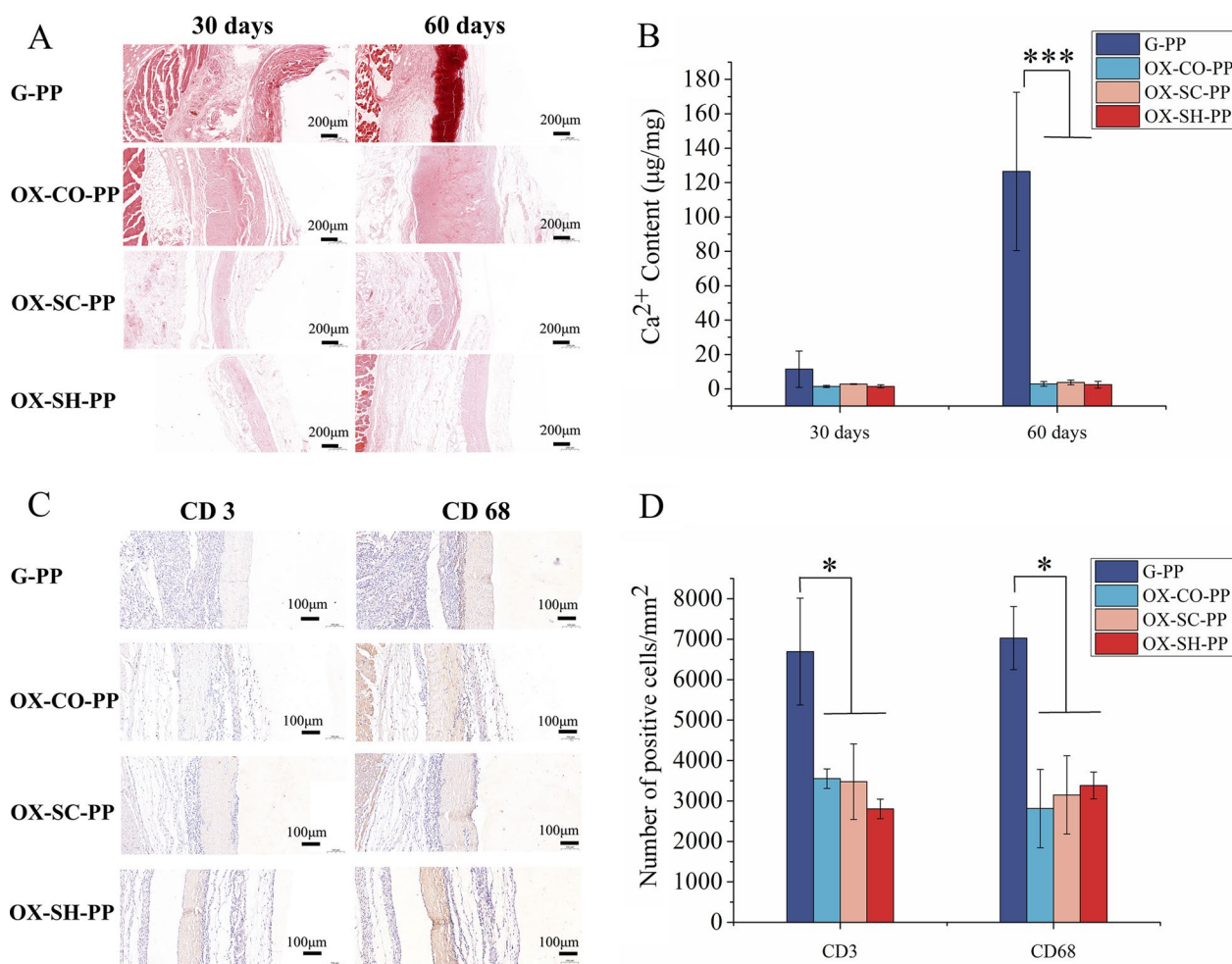


**Fig. 5** **A** Calcium contents of G-PP, OX-CO-PP, OX-SC-PP and OX-SH-PP after subcutaneous implantation in SD rats for 30 days and 60 days. (n = 6, \*\*\*p < 0.001). **B** Alizarin red stained sections of different cross-linked valve after implantation for 30 days and 60 days. (bar = 200 µm). **C** Immunohistochemistry with CD3 and CD 68 markers of different cross-linked valve after subcutaneous implantations in rats for 7 days. (bar = 100 µm). **D** The numbers of CD3-positive cells and CD68-positive cells aggregated around the specimens after implantation for 7 days

functional BHV materials along with the comparable mechanical property and collagen stability, making them a great potential for the bioprosthetic heart valve applications in clinic.

**Abbreviations**

- BHV Bioprosthetic artificial heart valve
- PP Porcine pericardium
- BP Bovine pericardium
- OX-CO Bicyclic oxazolidine with a carboxyl functional group
- D-PP Decellularized porcine pericardium
- G-PP Glutaraldehyde cross-linked porcine pericardium
- OX-CO-PP OX-CO cross-linked porcine pericardium
- OX-SC-PP Sulfated chitosan grafted OX-CO-PP
- OX-SH-PP Heparin sodium grafted cross-linked OX-SC-PP
- DSC Differential scanning calorimetry
- SEM Scanning electron microscopy
- FPP Frequency platelet plasma
- PT Prothrombin time

- APTT Active partial thrombin time
- ICP-AES Inductively coupled plasma-atomic emission spectrometry

**Supplementary Information**

The online version contains supplementary material available at <https://doi.org/10.1186/s42825-022-00098-z>.

**Additional file 1** Mass spectrometry of OX-CO; <sup>1</sup>H NMR and <sup>13</sup>C NMR spectra for OX-CO; Relative free amine content of PPs; Micromorphology of valves; FTIR spectrum and elemental content of 3,6-O-sulfated chitosan.

**Acknowledgements**

We would be grateful to the help of VENUS Medtech Inc. (Hangzhou, China) for providing the fresh porcine pericardium and the valuable comments and suggestions of the anonymous reviewers.

**Author contributions**

All authors have given approval to the final version of the manuscript.

### Funding

This research was financially supported by National Key Research and Development Programs (2020YFC1107802), the National Natural Science Foundation of China (32071357), the Sichuan Science and Technology Program (2021YFH0011), Sichuan Province Major Science and Technology Special Projects (2018SZDX0011), the National 111 project of Introducing Talents of Discipline to Universities (No. B16033). We would be grateful to the help of VENUS Medtech Inc. (Hangzhou, China) for providing the fresh porcine pericardium.

### Availability of data and materials

This manuscript contains all of the data generated or analyzed during this research.

### Declarations

#### Competing interests

The authors declare no competing financial interest.

#### Ethics approval and consent to participate

The use of animals and all protocols were approved by the by the Sichuan Provincial Committee for Experimental Animal Management (K2022020) and performed according to the institutional and NIH guidelines for the care and use of research animals.

#### Author details

<sup>1</sup>National Engineering Research Center of Clean Technology in Leather Industry, Sichuan University, Chengdu 610065, China. <sup>2</sup>National Engineering Research Center for Biomaterials, Sichuan University, Chengdu 610065, China. <sup>3</sup>Venus Medtech (Hangzhou) Inc., Hangzhou, China.

Received: 5 May 2022 Revised: 21 July 2022 Accepted: 4 August 2022

Published: 20 August 2022

### References

- Fioretta ES, Dijkman PE, Emmert MY, Hoerstrup SP. The future of heart valve replacement: recent developments and translational challenges for heart valve tissue engineering. *J Tissue Eng Regen Med*. 2018;12:e323–35.
- Eleid MF, Holmes DR. Transcatheter aortic valve replacement: state of the art and future directions. *Annu Rev Med*. 2017;68:15–28.
- Gales J, Krasuski RA, Fleming GA. Transcatheter valve replacement for right-sided valve disease in congenital heart patients. *Prog Cardiovasc Dis*. 2018;61:347–59.
- Wang Y, Li G, Yang L, Luo R, Guo G. Development of innovative biomaterials and devices for the treatment of cardiovascular diseases. *Adv Mater*. 2022. <https://doi.org/10.1002/adma.202201971>.
- Kostyunin AE, Yuzhalin AE, Rezvova MA, Ovcharenko EA, Glushkova TV, Kutikhin AG. Degeneration of bioprosthetic heart valves: update 2020. *J Am Heart Assoc*. 2020;9:1–19.
- Lameijer H, van Slooten YJ, Jongbloed MRM, Oudijk MA, Kampman MAM, van Dijk AP, Post MC, Mulder BJ, Sollie KM, van Veldhuisen DJ, Ebels T, van Melle JP, Pieper PG. Biological versus mechanical heart valve prosthesis during pregnancy in women with congenital heart disease. *Int J Cardiol*. 2018;268:106–12.
- Tam H, Zhang W, Infante D, Parchment N, Sacks M, Vyavahare N. Fixation of bovine pericardium-based tissue biomaterial with irreversible chemistry improves biochemical and biomechanical properties. *J Cardiovasc Transl Res*. 2017;10:194–205.
- Ma B, Wang X, Wu C, Chang J. Crosslinking strategies for preparation of extracellular matrix-derived cardiovascular scaffolds. *Regen Biomater*. 2014;1:81–9.
- Lee S, Kim DH, Youn YN, Joo HC, Yoo KJ, Lee SH. Rosuvastatin attenuates bioprosthetic heart valve calcification. *J Thorac Cardiovasc Surg*. 2019;158:731–41.
- Lopez-Moya M, Melgar-Lesmes P, Kollandaivelu K, De La Torre Hernández JM, Edelman ER, Balcells M. Optimizing glutaraldehyde-fixed tissue heart valves with chondroitin sulfate hydrogel for endothelialization and shielding against deterioration. *Biomacromol*. 2018;19:1234–44.
- Dangas GD, Weitz JI, Giustino G, Makkar R, Mehran R. Prosthetic heart valve thrombosis. *J Am Coll Cardiol*. 2016;68:2670–89.
- Lim WY, Lloyd G, Bhattacharya S. Mechanical and surgical bioprosthetic valve thrombosis. *Heart*. 2017;103:1934–41.
- Kalfa D. Novel valve choices for pulmonary valve replacement. *Semin Thorac Cardiovasc Surg*. 2022. <https://doi.org/10.1053/j.semctvs.2021.11.018>.
- McElhinney DB, Sondergaard L, Armstrong AK, Bergersen L, Padera RF, Balzer DT, Lung TH, Berger F, Zahn EM, Gray RG, Hellenbrand WE, Kreutzer J, Eicken A, Jones TK, Ewert P. Endocarditis after transcatheter pulmonary valve replacement. *J Am Coll Cardiol*. 2018;72:2717–28.
- Muñiz MT, Eiras M, Selas S, Garcia J. Loeffler endocarditis associated with a massive right intraventricular thrombus. *Intensive Care Med*. 2018;44:2296–7.
- Doris MK, Dweck MR. Is bioprosthetic leaflet thrombosis a trigger to valve degeneration? *Heart*. 2018;104:792–3.
- Senage T, Paul A, Le Tourneau T, Fella-Habia I, Vadori M, Bashir S, Galiñanes M, Bottio T, Gerosa G, Evangelista A, Badano LP, Nassi A, Costa C, Cesare G, Manji RA, Cueff C, de Monchy N, Piriou RC, Serfaty JM, Guimbretière G, Dantan E, Ruiz-Majoral A, Coste G, du Fou S, Ben-Arye L, Govani L, Yehuda S, Abramovitch SB, Amon R, Reuven EM, Atiya-Nasagi Y, Hai Y, Iop L, Casós K, Kuguel SG, Blasco-Lucas A, Permyer E, Sbraga F, Llatjós R, Moreno-Gonzalez G, Sánchez-Martínez M, Breimer ME, Holgersson J, Teneberg S, Pascual-Gilbert M, Nonell-Canals A, Takeuchi Y, Chen X, Mañez R, Roussel JC, Soullou JP, Cozzi E, Padler-Karavani V. The role of antibody responses against glycans in bioprosthetic heart valve calcification and deterioration. *Nat Med*. 2022;28(2):283–94. <https://doi.org/10.1038/s41591-022-01682-w>.
- Sanaani A, Yandrapalli S, Harburger JM. Antithrombotic management of patients with prosthetic heart valves. *Cardiol Rev*. 2018;26(4):177–86. <https://doi.org/10.1097/CRD.0000000000000189>.
- Mosarla RC, Vaduganathan M, Qamar A, Moslehi J, Piazza G, Giugliano RP. Anticoagulation strategies in patients with cancer: JACC review topic of the week. *J Am Coll Cardiol*. 2019;73:1336–49.
- Kang IK, Kwon OH, Kim MK, Lee YM, Sung YK. In vitro blood compatibility of functional group-grafted and heparin-immobilized polyurethanes prepared by plasma glow discharge. *Biomaterials*. 1997;18:1099–107.
- Gao J, Jiang L, Liang Q, Shi J, Hou D, Tang D, Chen S, Kong D, Wang S. The grafts modified by heparinization and catalytic nitric oxide generation used for vascular implantation in rats. *Regen Biomater*. 2018;5:105–14.
- Chanda J, Kuribayashi R, Abe T. Heparin in calcification prevention of porcine pericardial bioprostheses. *Biomaterials*. 1997;18:1109–13.
- Chow VCC, Pai RP, Chapman JR, O'Connell PJ, Allen RDM, Mitchell P, Nankivell BJ. Diabetic retinopathy after combined kidney-pancreas transplantation. *Clin Transplant*. 1999;13:356–62.
- Liu Z, Li G, Zheng Z, Li Y, Han Y, Kaplan DL, Wang X. Silk fibroin-based woven endovascular prosthesis with heparin surface modification. *J Mater Sci Mater Med*. 2018. <https://doi.org/10.1007/s10856-018-6055-3>.
- Wang X, Guan J, Zhuang X, Li Z, Huang S, Yang J, Liu C, Li F, Tian F, Wu J, Shu Z. Exploration of blood coagulation of N-alkyl chitosan nanofiber membrane in vitro. *Biomacromol*. 2018;19:731–9.
- Liu G, Xiang J, Xia Q, Li K, Yan H, Yu L. Fabrication of durably antibacterial cotton fabrics by robust and uniform immobilization of silver nanoparticles via mussel-inspired polydopamine/polyethyleneimine coating. *Ind Eng Chem Res*. 2020;59:9666–78.
- Vikhoreva G, Bannikova G, Stolbushkina P, Panov A, Drozd N, Makarov V, Varlamov V, Gal'braikh L. Preparation and anticoagulant activity of a low-molecular-weight sulfated chitosan. *Carbohydr Polym*. 2015;62:327–32.
- Yu T, Chen X, Zhuang W, Tian Y, Liang Z, Kong Q, Hu C, Li G, Wang Y. Non-glutaraldehyde treated porcine pericardium with good biocompatibility, reduced calcification and improved Anti-coagulation for bioprosthetic heart valve applications. *Chem Eng J*. 2021;414:128900.
- Yu T, Yang W, Zhuang W, Tian Y, Kong Q, Chen X, Li G, Wang Y. A bioprosthetic heart valve cross-linked by a non-glutaraldehyde reagent with improved biocompatibility, endothelialization, anti-coagulation and anti-calcification properties. *J Mater Chem B*. 2021;9:4031–8.
- Sélabarom J, Monge S, Carré F, Roque JP, Pavia AA. Stereoelectronic control of oxazolidine ring-opening: Structural and chemical evidences. *Tetrahedron*. 2002;58:9559–66.

31. Yuan L, Yue Z, Chen H, Huang H, Zhao T. Biomacromolecular affinity: Interactions between lysozyme and regioselectively sulfated chitosan. *Colloids Surfaces B Biointerfaces*. 2009;73:346–50.
32. Luo Y, Lou D, Ma L, Gao C. Optimizing detergent concentration and processing time to balance the decellularization efficiency and properties of bioprosthetic heart valves. *J Biomed Mater Res Part A*. 2019;107:2235–43.
33. Tardalkar K, Marsale T, Bhamare N, Kshersagar J, Chaudhari L, Joshi MG. Heparin immobilization of tissue engineered xenogeneic small diameter arterial scaffold improve endothelialization. *Tissue Eng Regen Med*. 2022;19(3):505–23. <https://doi.org/10.1007/s13770-021-00411-7>.
34. Hu C, Luo R, Wang Y. Heart valves cross-linked with erythrocyte membrane drug-loaded nanoparticles as a biomimetic strategy for anti-coagulation, anti-inflammation, anti-calcification, and endothelialization. *ACS Appl Mater Interfaces*. 2020;12:41113–26.
35. Lien SM, Ko LY, Huang TJ. Effect of pore size on ECM secretion and cell growth in gelatin scaffold for articular cartilage tissue engineering. *Acta Biomater*. 2009;5:670–9.
36. Yang F, He H, Xu L, Jin L, Guo G, Wang Y. Inorganic-polymerization crosslinked tissue-siloxane hybrid as potential biomaterial for bioprosthetic heart valves. *J Biomed Mater Res Part A*. 2021;109:754–65.
37. Chen G. The past ten years of carbohydrate polymers in ACS macro letters. *ACS Macro Lett*. 2021;10(9):1145–50. <https://doi.org/10.1021/acsmacrolett.1c00526>.
38. Ihsan AB, Koyama Y. Substituent optimization of (1 → 2)-Glucopyranan for tough, strong, and highly stretchable film with dynamic interchain interactions. *ACS Macro Lett*. 2020;9(5):720–4. <https://doi.org/10.1021/acsmacrolett.0c00266>.
39. Caracciolo PC, Diaz-Rodriguez P, Ardao I, Moreira D, Montini-Ballarin F, Abraham GA, Concheiro A, Alvarez-Lorenzo C. Evaluation of human umbilical vein endothelial cells growth onto heparin-modified electrospun vascular grafts. *Int J Biol Macromol*. 2021;179:567–75.
40. Fazil S, Shah H, Noreen M, Yar M, Farooq Khan A, Zaman Safi S, Yousef Alomar S, Fahad Alkharji A, Mualla Alharbi H, Sohail AM. Evaluation of molecular mechanisms of heparin-induced angiogenesis, in human umbilical vein endothelial cells. *J King Saud Univ Sci*. 2021;33: 101534.
41. Marcum JA, McKenney JB, Rosenberg RD. Acceleration of thrombin-antithrombin complex formation in rat hindquarters via heparinlike molecules bound to the endothelium. *J Clin Invest*. 1984;74:341–50.
42. Moghimi SM, Simberg D. Complement activation turnover on surfaces of nanoparticles. *Nano Today*. 2017;15:8–10.

### Publisher's Note

Springer Nature remains neutral with regard to jurisdictional claims in published maps and institutional affiliations.

Submit your manuscript to a SpringerOpen<sup>®</sup> journal and benefit from:

- Convenient online submission
- Rigorous peer review
- Open access: articles freely available online
- High visibility within the field
- Retaining the copyright to your article

---

Submit your next manuscript at ► [springeropen.com](https://www.springeropen.com)

---